flocculation and sedimentation.

Although this model is open to improvement (for example, the vertical dimension and the nature and characteristics of the bottom are not included), it can yet provide valuable information for similar studies as well as for models involving biological processes.

REFERENCES

Beckers, O. and Wollast, R., 1977. Comportement de la silice dissoute dans l'estuaire de l'Escaut. In : J.C.J. Nihoul and R. Wollast (Editors), l'Estuaire de l'Escaut, Vol. 10, Projet Mer. La Politique Scientifique, Bruxelles, pp. 153-170.

Billen, G., Smitz, J., Somville, M. and Wollast, R., 1977. Dégradation de la matière organique et processus d'oxydo-réduction dans l'estuaire de l'Escaut. In : J.C.J. Nihoul and R. Wollast (Editors), l'Estuaire de l'Escaut, Vol. 10, Projet Mer. La Politique Scientifique, Bruxelles, pp. 102-152.

Cormault, P., 1971. Détermination expérimentale du débit solide d'érosion de sédiments fins cohésifs. Proc. 14th Congress IAHR, Paris, 4 : 9-16.

Elder, J.W., 1959. The dispersion of marked fluid in turbulent shear flow. J. Fluid Mech., 5 : 544.

Hjulstrom, F., 1935. Studies of the morphological activity of rivers as illustrated by the river Fyris. Bull. Geol. Inst. Uppsala, 25 : 221-527.

Leendertse, J.J. and Gritton, E.C., 1971a. A water-quality simulation model for well mixed estuaries and coastal seas, Vol. II, Computational procedures. The Rand Corporation, 53 pp.

Leendertse, J.J. and Gritton, E.C., 1971b. A water-quality simulation model for well mixed estuaries and coastal seas, Vol. III, Jamaica Bay simulation. The Rand Corporation, 73 pp.

Migniot, Cl., 1968. Etude des propriétés physiques de différents sédiments très fins et de leur comportement sous des actions hydrodynamiques. La Houille Blanche, 7 : 591-620.

Nihoul, J.C.J., 1975. Hydrodynamic Models. In : J.C.J. Nihoul (Editor), Modelling of Marine Systems, Oceanography Series No 10. Elsevier, Amsterdam, pp 41-67.

Nihoul, J.C.J. and Adam, Y., 1975. Dispersion et sédimentation autour d'un point de déversement en mers peu profondes, J. Hydr. Res., 13 : 171.

Wartel, S., 1971a. Bepalen van wrijvingssnelheden tegen de bodem op basis van stroomsnelheidsverticalen. Koninklijk Belgisch Instituut voor Natuurwetenschappen, Brussels, 21 pp.

Wartel, S., 1971b. Studie van het flokulatieproces op Schelde sedimenten, Koninklijk Belgisch Instituut voor Natuurwetenschappen, Brussels, 15 pp.

Wartel, S., 1972. Sedimentologisch onderzoek van de opbouw van het Schelde-estuarium. Doctorate's thesis, Leuven, Vol. III, 188 pp.

Wollast, R., 1973. Origine et mécanisme de l'envasement de l'estuaire de l'Escaut. Rapport de Synthèse, Ministère des Travaux Publics, Borgerhout, 140 pp.

Wollast, R., 1977. Transport et accumulation de polluants dans l'estuaire de l'Escaut. In : J.C.J. Nihoul and R. Wollast (Editors), l'Estuaire de l'Escaut, Vol. 10, Projet Mer. La Politique Scientifique, Bruxelles, pp. 191-218.

Reprinted from *Ecohydr* ...amics*, edited by J.C.J. Nihoul

NUMERICAL SIMULATIONS OF SALINITY, TURBIDITY AND SEDIMENT ACCUMULATION IN THE SCHELDT ESTUARY

W. BAEYENS[1], Y. ADAM[2], J.P. MOMMAERTS[2] and G. PICHOT[2]

[1]Dienst Analytische Scheikunde, Vrije Universiteit Brussel, Brussels (Belgium)

[2]Beheerseenheid Model Noordzee en Schelde, Ministerie van Volksgezondheid en Leefmilieu, Brussels (Belgium)

ABSTRACT

In order to simulate the physical behaviour of the Scheldt estuary, a hydrodynamic and a dispersion model have been devised. Both models are two dimensional, vertically integrated, and are solved numerically with a multioperational finite difference scheme, using a grid of 300 x 300 meters. The hydrodynamic model, which allows the simulation of instantaneous water levels and mean velocities over depth is controlled at the downstream boundary by time-varying water levels and at the upstream boundary by the river flow. The dispersion model, which predicts the evolution of salinity and turbidity in the water column and the sedimentary budget at the bottom, is controlled at the upstream and the downstream boundary by time-varying salinity values dependent on the river flow and by time-varying turbidity values averaged over the river flow.

An increase of the river flow causes a downstream shift of the brackish water zone. Due to the influence of the salinity on flocculation and therefore on sedimentation of suspended material, the sedimentation zone is also shifted downstream. This results in higher turbidities and a lower sedimentary budget at the bottom in the upstream part of the estuary.

Under average hydrodynamic conditions the computed sedimentary budget integrated over a tidal cycle at the different grid points agrees well with observations of mud accumulation in the same area.

INTRODUCTION

The physical behaviour of the Scheldt estuary i.e. the flow of water, salts and particulate matter, has a great influence on the dynamics of the ecosystem (growth of living organisms, transport of heavy metals, etc.). For instance, the heterotrophic bacterial activity is very high in the upstream part of the Scheldt estuary but drops dramatically at about 60 km from the river mouth (G. Billen et

al., 1977). This drop has been explained by the effect of increased salinity which causes (1) flocculation of suspended matter and organic matter and subsequent sedimentation, (2) inhibition of the activity of the fresh water bacteria. Considering the dynamics of phytoplankton, primary production is controlled by the incident light and the transparency of the water which can be inferred from the turbidity. As soon as the intensity of the incident light is sufficient to ensure photosynthesis, the development of diatoms starts at the mouth of the estuary where the turbidity is minimum (O. Beckers and R. Wollast, 1977). During summer the area of development progressively moves upstream as a result of an increasing light intensity and an exhaustion of silica in the downstream part of the estuary.

It is obvious from the few examples mentioned above, that a sound understanding of estuarine physics is a prerequisite for all concerned with the dynamics of estuarine ecosystems. Unfortunately, the complex geometry of the estuary (ebb and flood channels, tidal flats, meanders) as well as non-tidal fluctuations of the hydrodynamic boundaries (river flow and tidal amplitude range from 10 m^3/s to 400 m^3/s and from 2.96 m to 4.42 m respectively) make the description and prediction of the velocity field and hence of the dispersion of salinity and turbidity very difficult. Moreover, the behaviour of the turbidity is strongly depending on direct and indirect interactions with the other physical variables. Flocculation of the fine grained material supplied by the river starts as soon as the salinity exceeds 1 $^{o}/_{oo}$. This flocculation zone has no fixed position but moves to and fro during a tidal cycle. In periods of high (low) river flow and decreasing (increasing) tidal amplitude at the mouth, the tidal flocculation zone is shifted downstream (upstream). Local hydrodynamic conditions govern the settling down of the flocculated material. Considering the annual amount of material accumulating at the bottom in various areas of the Scheldt estuary (Wollast, 1977), two distinct sedimentation zones can be defined. In the area Rupelmonde (km 90) - Doel (km 60) the accumulation amounts to 2000 10^3 tons/year and in the area Doel (km 60) - Hansweert (km 35) it amounts to 220 10^3 tons/year (these values only reflect the balance of sedimentation and erosion).

In order to gain better insight in processes such as flocculation, sedimentation and erosion and consequently in the interactions between the physical variables, we decided to construct a mathematical model which should enable us to simulate these phenomena and to predict the evolution in space and time of the selected variables. It should also allow to calculate local sedimentary budgets.

MATHEMATICAL EQUATIONS : HYDRODYNAMICS

In shallow seas as well as in well-mixed estuaries it is generally sufficient to consider depth-averaged variables. The momentum and continuity equations governing the dynamics of the fluid after integration over the depth become :

$$\frac{\partial \underline{V}}{\partial t} + \underline{V} \cdot \nabla_h \underline{V} + f e_z \wedge \underline{V} + g \nabla_h \zeta = \nu \nabla_h^2 \underline{V} + (\tau_s - \tau_b) / \rho H \qquad (1)$$

$$\frac{\partial H}{\partial t} + \nabla_h \cdot \underline{V} H = 0 \qquad (2)$$

$$\underline{V} = \frac{1}{H} \int_{-h}^{\zeta} \underline{v} \, dz \qquad (3)$$

with :

$\underline{v}$	velocity vector
$\underline{V}$	mean velocity vector over depth
∇_h	gradient in horizontal directions
f	Coriolis factor
e_z	unit vector in the vertical direction
g	gravitational acceleration
ζ	surface water level relative to the reference plane
h	distance from the reference plane to the bottom
H	total depth
ν	viscosity coefficient
τ_s, τ_b	surface and bottom stresses
ρ	fluid density

DEFINITION OF THE CONTROL PARAMETERS

The three control parameters ν, τ_s and τ_b in equation (1) need to be specified.

As the viscosity term includes in fact two effects : on the one hand eddy viscosity caused by erratic small scale motions and on the other hand shear turbulence due to the inhomogeneous vertical velocity field, the overall viscosity coefficient (ν) is the sum of the eddy (ν_e) and the shear viscosity coefficient (ν_s). According to Kolmogorov's theory, ν_e equals 5 m^2/s, while an estimation of ν_s on the basis of Nihoul's work (Nihoul, 1975) gave a value of 20 m^2/s. Hence ν equals about 25 m^2/s.

The shear stress at the surface (τ_s) can become significant in periods of very strong winds, but is generally very small in estuaries compared with the shear stress at the bed (τ_b). Therefore τ_s is not included in the model.

By definition, bottom stress and shear velocity (V_*) are related as follows :

$$V_* = (\tau_b / \rho)^{1/2} \qquad (4)$$

However, in two dimensional, vertically integrated models, the shear stress must be inferred from the mean velocity over depth. Often the following expression is used :

$$\tau_b = \rho D \underline{V} \, | \underline{V} | \qquad (5)$$

where D is a drag coefficient, dependent on the roughness of the channel bed. In

al., 1977). This drop has been explained by the effect of increased salinity which causes (1) flocculation of suspended matter and organic matter and subsequent sedimentation, (2) inhibition of the activity of the fresh water bacteria. Considering the dynamics of phytoplankton, primary production is controlled by the incident light and the transparency of the water which can be inferred from the turbidity. As soon as the intensity of the incident light is sufficient to ensure photosynthesis, the development of diatoms starts at the mouth of the estuary where the turbidity is minimum (O. Beckers and R. Wollast, 1977). During summer the area of development progressively moves upstream as a result of an increasing light intensity and an exhaustion of silica in the downstream part of the estuary.

It is obvious from the few examples mentioned above, that a sound understanding of estuarine physics is a prerequisite for all concerned with the dynamics of estuarine ecosystems. Unfortunately, the complex geometry of the estuary (ebb and flood channels, tidal flats, meanders) as well as non-tidal fluctuations of the hydrodynamic boundaries (river flow and tidal amplitude range from 10 m^3/s to 400 m^3/s and from 2.96 m to 4.42 m respectively) make the description and prediction of the velocity field and hence of the dispersion of salinity and turbidity very difficult. Moreover, the behaviour of the turbidity is strongly depending on direct and indirect interactions with the other physical variables. Flocculation of the fine grained material supplied by the river starts as soon as the salinity exceeds 1 $^{o}/_{oo}$. This flocculation zone has no fixed position but moves to and fro during a tidal cycle. In periods of high (low) river flow and decreasing (increasing) tidal amplitude at the mouth, the tidal flocculation zone is shifted downstream (upstream). Local hydrodynamic conditions govern the settling down of the flocculated material. Considering the annual amount of material accumulating at the bottom in various areas of the Scheldt estuary (Wollast, 1977), two distinct sedimentation zones can be defined. In the area Rupelmonde (km 90) - Doel (km 60) the accumulation amounts to 2000 10^3 tons/year and in the area Doel (km 60) - Hansweert (km 35) it amounts to 220 10^3 tons/year (these values only reflect the balance of sedimentation and erosion).

In order to gain better insight in processes such as flocculation, sedimentation and erosion and consequently in the interactions between the physical variables, we decided to construct a mathematical model which should enable us to simulate these phenomena and to predict the evolution in space and time of the selected variables. It should also allow to calculate local sedimentary budgets.

MATHEMATICAL EQUATIONS : HYDRODYNAMICS

In shallow seas as well as in well-mixed estuaries it is generally sufficient to consider depth-averaged variables. The momentum and continuity equations governing the dynamics of the fluid after integration over the depth become :

$$\frac{\partial \underline{V}}{\partial t} + \underline{V} \cdot \nabla_h \underline{V} + f e_z \wedge \underline{V} + g \nabla_h \zeta = \nu \nabla_h^2 \underline{V} + (\tau_s - \tau_b) / \rho H \qquad (1)$$

$$\frac{\partial H}{\partial t} + \nabla_h \cdot \underline{V} H = 0 \qquad (2)$$

$$\underline{V} = \frac{1}{H} \int_{-h}^{\zeta} \underline{v} \, dz \qquad (3)$$

with :

$\underline{v}$	velocity vector
$\underline{V}$	mean velocity vector over depth
∇_h	gradient in horizontal directions
f	Coriolis factor
e_z	unit vector in the vertical direction
g	gravitational acceleration
ζ	surface water level relative to the reference plane
h	distance from the reference plane to the bottom
H	total depth
ν	viscosity coefficient
τ_s, τ_b	surface and bottom stresses
ρ	fluid density

DEFINITION OF THE CONTROL PARAMETERS

The three control parameters ν, τ_s and τ_b in equation (1) need to be specified.

As the viscosity term includes in fact two effects : on the one hand eddy viscosity caused by erratic small scale motions and on the other hand shear turbulence due to the inhomogeneous vertical velocity field, the overall viscosity coefficient (ν) is the sum of the eddy (ν_e) and the shear viscosity coefficient (ν_s). According to Kolmogorov's theory, ν_e equals 5 m^2/s, while an estimation of ν_s on the basis of Nihoul's work (Nihoul, 1975) gave a value of 20 m^2/s. Hence ν equals about 25 m^2/s.

The shear stress at the surface (τ_s) can become significant in periods of very strong winds, but is generally very small in estuaries compared with the shear stress at the bed (τ_b). Therefore τ_s is not included in the model.

By definition, bottom stress and shear velocity (V_*) are related as follows :

$$V_* = (\tau_b / \rho)^{1/2} \qquad (4)$$

However, in two dimensional, vertically integrated models, the shear stress must be inferred from the mean velocity over depth. Often the following expression is used :

$$\tau_b = \rho D \underline{V} \, || \underline{V} || \qquad (5)$$

where D is a drag coefficient, dependent on the roughness of the channel bed. In

hydraulic engineering extensive use is made of Chezy's formulation :

$$D = g/C^2 \qquad (6)$$

with C the Chezy coefficient. From vertical velocity profiles and corresponding shear velocities (see SOURCES AND SINKS), we deduced for the bottom of the Scheldt estuary a typical friction coefficient (Manning's n) of $3.3\ 10^{-2}$.

NUMERICAL METHOD AND BOUNDARY CONDITIONS

The partial differential equations (1) and (2) are approximated by two finite difference equations, one explicit the other implicit, used alternatively for a step by step solution in time. The advantage of such a procedure is that over a whole time step the different terms in equations (1) and (2) are either central in time or averaged over that time interval, allowing less severe stability conditions concerning the time step.

This scheme is very close to Leendertse's (Leendertse et al., 1971a) multi-operation method. Only the advection terms are calculated on a higher time level by an iterative procedure, and the viscosity term, which is added to the momentum equation is calculated explicitly.

The calculations are carried out with a 300 x 300 m mesh-size grid (Figure 1). The downstream boundary is situated at 45 km from the mouth, the upstream boundary at 120 km from the mouth. From km 65 on, the Scheldt becomes so narrow (about 500 to 600 meters), that we have "straightened" the river, leaving its cross-sectional geometry (width, depth, tidal flat) unchanged. The global time step equals 2 minutes.

As one of our objectives requires a mean hydrodynamic situation, the following boundary conditions are used :

- Downstream : a mean input tide
- Upstream : a mean ($Q = 80\ m^3/s$), a high ($Q = 350\ m^3/s$) and a low ($Q = 1\ m^3/s$) river flow

The initial conditions (velocities are zero and the water level equals the low water level at the downstream boundary) do not have any influence on the final results, because simulations are carried out until a cyclic pattern (generally after three tides) is obtained.

RESULTS

In order to simulate flooding of tidal flats during rising tide and subsequent retreating of the land-water boundary during ebb, an adapted numerical procedure was used. To illustrate this procedure, the various dry (circles) and wet grid points (intersections) at low water are represented on Figure 1.

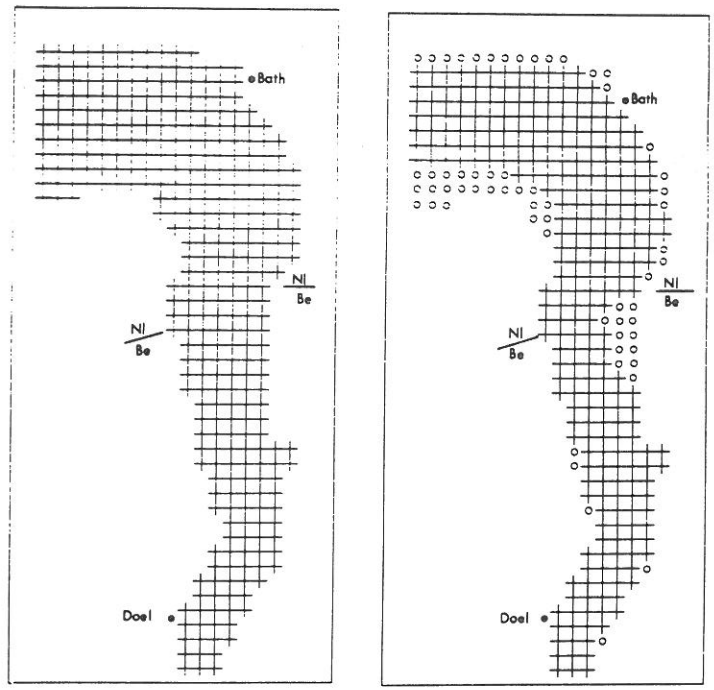

Fig. 1 : The numerical grid at high water (on the left) and at low water (on the right). The dry grid points at low water are indicated by circles.

The agreement between measured and computed tide levels is very good. But achieving a good agreement between measured and computed velocities, and possibly adjusting the model accordingly, is of course more important for constituent transport simulations. This is, however, a very difficult task, because one needs reliable data on instantaneous mean velocities over depth, for the hydrodynamic boundary conditions used in this model (mean input tide, mean river flow). Although we were not able to compare the calculated velocities with field data, two facts suggested the calculated velocity field was realistic : (1) with a comparable hydrodynamic model of Jamaica Bay, Leendertse et al. (1971b) observed a fairly good agreement between their calculated and measured data ; (2) we calculated the water mass transport through four cross sections and found that agreement with observed data was good (Ministère des Travaux Publics, personal communication) and that the law of conservation of total fluid mass was satisfied.

From the computed velocity patterns at different moments of the tide, it is clear that most of the time very high velocities occur in the channels, whereas in the shallow parts, the velocities are much lower, causing large velocity gradients on a local scale. Small velocities are only observed half an hour before

high water and at the moment of current inversion is shown on Figure 2.

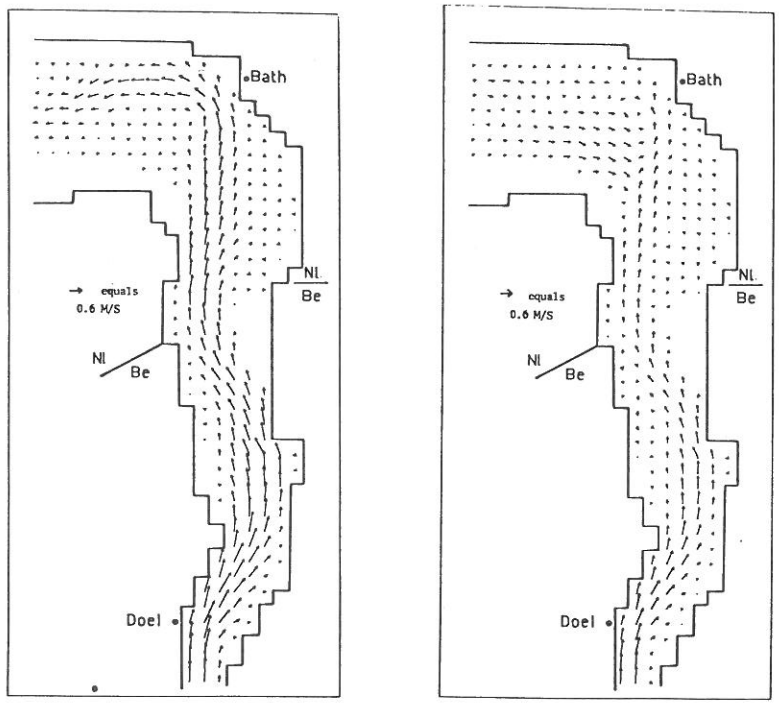

Fig. 2 : The calculated velocity pattern one hour before high water (on the left) and at the turn of the current (on the right).

Finally, velocity patterns were calculated for the three different river flows. Very small differences in local velocities were observed, confirming that the instantaneous velocities are almost entirely due to the tidal action.

MATHEMATICAL EQUATIONS : DISPERSION

The evolution of suspended solid matter and salinity can be described by their mass conservation equation. This equation is integrated over depth.

$$\frac{\partial HP}{\partial t} + \nabla_h \cdot H\underline{V}P = D_\alpha + HR + HS \qquad (7)$$

with : P concentration of constituent P

R interaction term (production-destruction rate of P by interactions with other constituents)

S source - sink term (input - output rate of P)

D_α diffusion term

As the velocity field is known, only the terms in the right hand side of equation (7) must be specified :

DIFFUSION (D_α)

The global diffusion takes into account eddy diffusion and shear diffusion. The eddy diffusion coefficient (λ_e) can be calculated in a way analogous to the eddy viscosity coefficient and equals 5 m^2/s.

It appears from the studies of Elder (1959) and Nihoul et al. (1975) that the magnitude of shear diffusion is proportional to the velocity and depth and that it acts in the same direction as the velocity vector. Hence, we expressed the shear diffusion coefficient (λ_s) as :

$$\lambda_s \sim VH\sqrt{g}/C \qquad (8)$$

The global diffusion coefficient (λ) is then the sum of λ_e which is isotropic, and λ_s, which is anisotropic.

INTERACTIONS (HR)

While the salinity is a passive constituent (other constituents have no influence on its evolution), biological and chemical reactions could produce or eliminate certain specific compounds of the suspended matter. This would result in a substantial modification of the solid matter composition in time and space. Such a modification, however, was not observed by Wollast (1973). His results, on the contrary, indicate a remarkably constant composition in the major elements. As the concentration of suspended matter is not affected by such interactions, these terms were not considered in the model.

SOURCES AND SINKS (HS)

This term includes sewage and industrial outfalls as well as interactions with the bottom sediments.

The outfalls are actually spread over a large part of the upstream estuary. As the simulation model cannot represent channels with a dimension smaller than the mesh-size, the lateral inputs are grouped at four locations. At each discharge point the flux of suspended matter, based on regular surveys, equals 250 kg particulate matter/minute.

The interaction between the water column and the bottom involves erosion and sedimentation. The sedimentation flux depends on the sedimentation velocity of the particles and the turbulence or shear stress at the bottom. When a viscous bottom layer is maintained on the estuarine floor, the flux of material is simply due to the slow sedimentation of particles. To allow for the periodic disruption of the viscous layer and ejection of sediments, a correcting factor, which is

related to the degree of sublayer instability, is introduced :

$$. S = -\frac{\sigma P}{H} (1 - \tau_b / \tau_c) \qquad \tau_b < \tau_c \qquad (9)$$

with : S sedimentation flux
σ sedimentation velocity
P suspended matter concentration or turbidity
H total depth
τ_b bottom shear stress
τ_c limiting shear stress above which no deposition takes place

Studies on flocculation processes, particle size distribution and sedimentation velocities (Wartel, 1971b ; Migniot, 1968) allowed us to derive the following relation between σ (meters/minute) and salinity (m S) :

$$. \sigma = 1.6\ 10^{-2} \qquad \text{Sal.} > 10 \text{ m S} \qquad (10)$$

$$. \sigma = 1.6\ 10^{-2} - 1.1\ 10^{-2} (10 - \text{Sal.})/8 \qquad \text{Sal.} < 10 \text{ m S} \qquad (11)$$

To express the bottom shear stress or the shear velocity - both of which are related according to equation (4) - in terms of the mean velocity over the depth, the vertical velocity profiles must be known. In the Scheldt river Wartel (1971a) found generally a very good agreement between the vertical velocity distribution and the Von Karman-Prandtl equation. Ratio's of shear velocity : mean velocity over depth, lay for a broad range of mean velocities (0.14 m/s to 1.60 m/s) between 0.06 and 0.07. This mean that in first approximation the ratio shear velocity : critical shear velocity can be replaced by mean velocity : critical mean velocity ;

$$. \tau_b/\tau_c = |\underline{V}|^2/V_c^2 \qquad (12)$$

with V_c about 0.7 m/s, based on simultaneous measurements of velocity and turbidity at 1 m above the bottom (Wartel, 1972).

Similar to the sedimentation flux, the erosion flux may be expressed as :

$$. S = \frac{M}{H} (1 - \tau_b / \tau_e) \qquad \tau_b > \tau_e \qquad (13)$$

with : S erosion flux
M mass of sediments removed per unit bed area and per unit time
τ_e critical erosion velocity

After replacing τ_c by τ_e relation (12) is also valid here. A critical erosion velocity of 0.7 m/s has been used.

Data for M were found in the literature (Cormault, 1971). For a similar sediment concentration (200 g/l) a value of 12 g/m^2/minute looked realistic. The adjustment of the model concerning the mean sedimentary budget (see RESULTS - SEDIMENTARY BUDGET) necessitated, however, different M values for downstream and upstream sections.

NUMERICAL METHOD AND BOUNDARY CONDITIONS

The numerical scheme used to solve equation (7) is also an explicit - implicit multioperation method. The numerical grid is the same as for the hydrodynamical calculations, but the model is now bounded upstream at Rupelmonde (km 90). The global time step is increased to 8 minutes. Calculations are carried out until a cyclic pattern is obtained (in general after three tidal periods). The computation starts with an initial salinity and turbidity gradient, in order to reduce the number of tides.

According to field measurements carried out at the downstream and upstream boundary of the model, we imposed at each boundary the following conditions :

- time-varying salinity values dependent on the river flow (both variables were inversely correlated) ;
- time-varying turbidity values averaged over the riverflow (both variables showed no correlation).

RESULTS - WATER COLUMN

The agreement between calculated and measured salinity profiles for a river flow of 80 m^3/s at km 45, 55 and 65 from the mouth is fairly good (Figure 3).

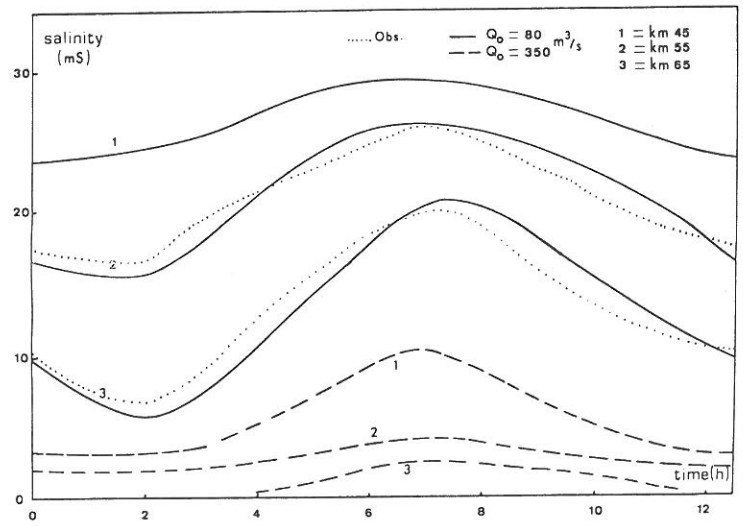

Fig. 3 : Calculated and measured salinity profiles, at three locations, for a mean and a high river flow.

The salinity profiles for a river flow of 350 m^3/s at the same locations are much lower than for a mean river flow (80 m^3/s), due to a downstream shift of the

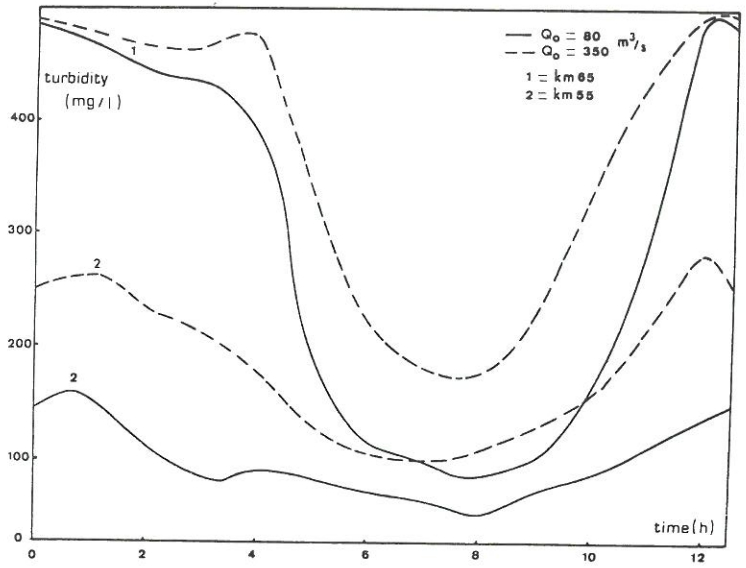

Fig. 4 : Calculated turbidity profiles, at two locations, for a mean and a high river flow.

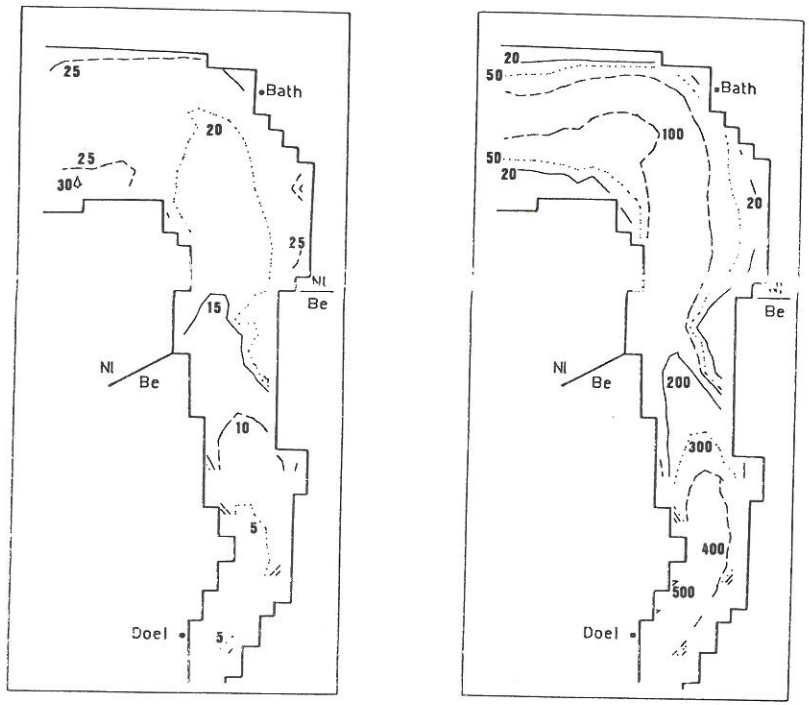

Fig. 5 : The calculated iso-concentration curves of salinity (on the left) and of turbidity (on the right) at low water for a mean river flow.

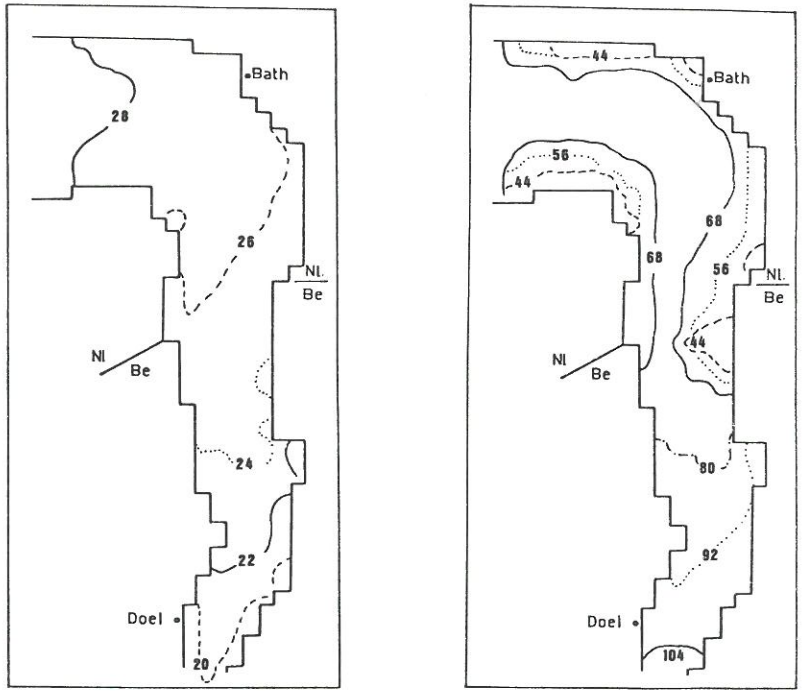

Fig. 6 : The calculated iso-concentration curves of salinity (on the left) and of turbidity (on the right) at high water for a mean river flow.

The calculated turbidity profiles for a river flow of 80 m^3/s at 55 and 65 km from the mouth, are on the other hand much lower than those obtained for a high river flow (Figure 4). As (1) the boundary conditions for the turbidity are identical for both river flows, and (2) the instantaneous velocities show only minor differences the much higher turbidity profiles observed in the case of high river flow at 55 and 65 km from the mouth are due to a downstream shift of the brackish water zone, and the influence of the salinity on flocculation and therefore on sedimentation of suspended material. The sedimentation zone is thus also shifted downstream resulting in higher turbidities in the upstream area.

The spatial patterns of salinity and turbidity respectively obtained at low (Figure 5) and at high water (Figure 6) illustrate the quite different behaviour of both variables. As the salinity is a passive variable, small gradients are locally observed. On the contrary, large variations in erosion-sedimentation fluxes between neighbouring points, cause very large turbidity gradients on a local scale, which are not at all compensated by turbulent diffusions.

Furthermore, whilst the salinity is strongly correlated with the tide, the turbidity shows no clear relationship with the tide because different inputs are

RESULTS - SEDIMENTARY BUDGET

A few tests on the sensitivity of the control parameters - σ, τ_c, τ_e and M - revealed that the yield coefficient M must be modified to give better agreement with the mean annual sedimentary budget estimated by Wollast (1977). By assigning lower M values to the upstream sediments than to the downstream sediments, we obtained the following results :

TABLE 1

Mean annual sedimentary budget

	Upstream area	Downstream area
(Wollast, 1977)	120 kg/m^{2}year	2 kg/m^{2}year
Model	90.6 kg/m^{2}year	- 1.7 kg/m^{2}year

The variability in the nature of the bottom sediments (in the upstream area, for example, the Scheldt is incised in the Boom clay which is very cohesive) probably explains the differences for the erosion yield coefficient (Hjulstrom, 1935).

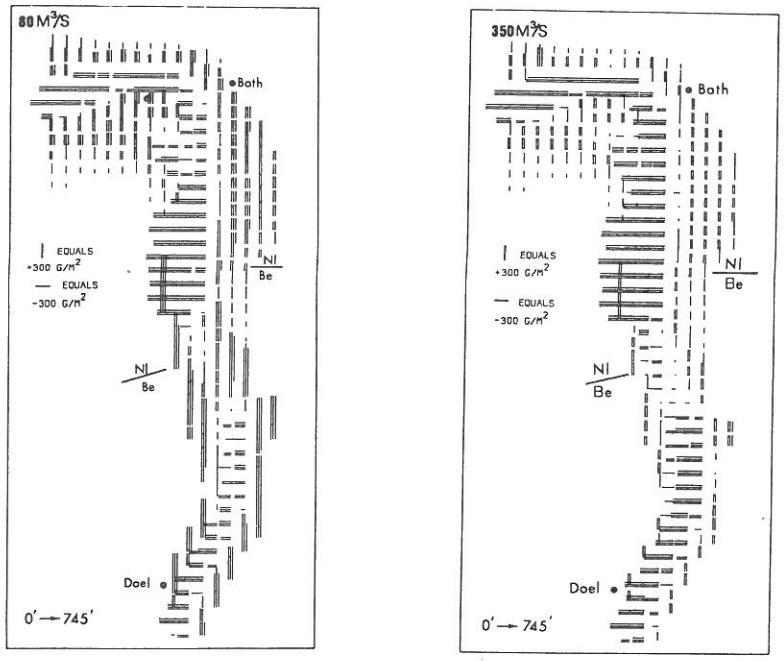

Fig. 7 : The sedimentary budget distribution, integrated over a tidal cycle, for a mean river flow (on the left) and for a high river flow (on the right)

The integrated sedimentary budget over a tidal period in the various grid points for a mean river flow and a river flow of 350 m^3/s (Figure 7) clearly suggest net erosion in the channels and sedimentation in the shallow areas.

The lower sedimentary budget obtained for high river flow, is caused by a downstream shift of the flocculation zone as explained in the previous section for the turbidity profiles.

At an arbitrarily choosen grid point we compared the evolution of the sedimentary budget during a tidal period for a mean river flow, with that obtained for a high river flow (Figure 8). As soon as the velocity falls beneath the critical sedimentation velocity, the budget increases, but at a much faster rate in the case of a mean river flow. When the velocity exceeds the critical erosion velocity the budget decreases in a similar way for both river flows. Finally, at the choosen grid point, the integrated budget shows a net erosion even for the lower river flow.

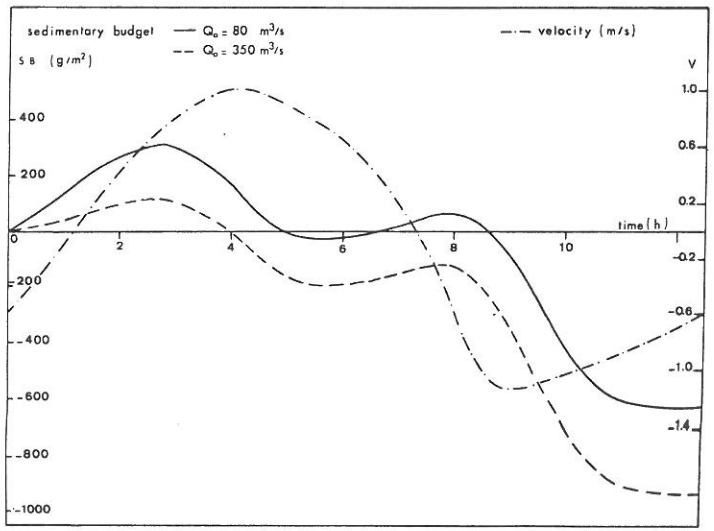

Fig. 8 : The evolution of the sedimentary budget during a tidal cycle, at an arbitrarily choosen grid point, for a mean and a high river flow.

CONCLUSIONS

The mathematical model presented here is capable of simulating the evolution of salinity, turbidity and the sedimentary budget at the bottom in a realistic way. The values attributed to the control parameters (σ, τ_e, τ_c, M) in the turbidity model, agreed fairly well with those determined by field measurements. Quite different turbidity profiles and sedimentary budgets at the bottom were obtained for low and high river flow due to the influence of the salinity on